Optical performance of holographic kinoforms

Dale A. Buralli, G. Michael Morris, and John R. Rogers

The optical properties of holographic kinoforms are described. It is shown that paraxial designs are not adequate for f/Nos. less than $\sim F/10$. A nonparaxial design is introduced that retains the high diffraction efficiency of the paraxial designs, yet also produces an unaberrated diffracted wavefront for the design wavelength. Aberration calculations and computer calculations, based on the Huygens-Fresnel principle, of the point spread functions for these elements show the necessity of using the nonparaxial design. Specifications for a surface profile that takes account of the finite thickness of the diffracting surface are given. A model for kinoforms which can be used in optical design programs is proposed.

I. Introduction

The kinoform is a phase hologram in which the phase modulation is introduced by a surface relief profile.[1] In most kinoforms, the maximum relief depth is chosen such that, at the chosen design wavelength, the maximum phase modulation introduced by the kinoform is 2π. Similar to other types of holograms, it is possible to use kinoforms as lenses.[2] In this paper we are concerned with rotationally symmetric kinoform lenses. Several precursors to the kinoform may be found in the literature. These devices go by various names, including phase plates[3,4] and phase Fresnel lenses.[5] Even though these kinoform lenses are based on the well-known principles of Fresnel zones, we will not use the term Fresnel lens to describe these devices, since Fresnel lens, in the field of optical design, usually refers to an optical element which utilizes incoherent superposition to form an image, while kinoforms rely on coherent imagery. The reader should be forewarned however, that this choice of terminology is far from uniform in the literature concerning these elements. We review the design of kinoform lenses in the paraxial approximation and then extend the design to the nonparaxial case. The optical peformance of the two designs, as functions of both wavelength and f/No. are compared. Also, we show what modifications to the diffracting surface are required to account for the effects of the finite thickness of the surface. We conclude with a suggestion concerning the modeling of these devices when used with conventional optical design programs.

When this work was done all authors were with University of Rochester, Institute of Optics, Rochester, New York 14627; J. R. Rogers is now with Wild-Leitz, Heerbrugg, Switzerland.

Received 19 May 1988.
0003-6935/89/060976-08$02.00/0.

II. Paraxial Kinoform Design

As a first step in describing the kinoform optical element, we shall model the device as an infinitely thin phase screen. Since the kinoform is a pure phase hologram, the transmission function is a unit magnitude, complex-exponential function. In the paraxial approximation, a rotationally symmetric lens is described by a transmission function that has a quadratic dependence on the radial coordinate,[6] i.e.,

$$t_{\text{lens}}(x,y;\lambda) = \exp\left[\frac{-i\pi(x^2+y^2)}{\lambda f}\right]. \tag{1}$$

In Eq. (1), x and y are the coordinates in the plane of the thin lens, λ is the wavelength of the light, and f is the focal length of the lens. We would like the kinoform to perform the same function as a lens, thus we expect the kinoform to have a transmission function similar to that in Eq. (1).

We recall that the Fresnel full-period zones are defined such that the optical path length from the edge of the mth zone is equal to $f + m\lambda_0$, where λ_0 is the wavelength for which the zones are defined. Thus, the equation that defines the locations of the zones in the x-y plane ($r^2 = x^2 + y^2$) is

$$r_m^2 = 2m\lambda_0 f + (m\lambda_0)^2. \tag{2}$$

In the paraxial region, $r^2 \ll (f/m)^2$, so Eq. (2) reduces to

$$r_{m,\text{paraxial}}^2 = 2m\lambda_0 f. \tag{2'}$$

We are therefore led to try a kinoform surface profile that has a zone spacing dictated by Eq. (2′) and a surface relief profile (blaze) that is parabolic within each zone. The surface profile is obtained from the desired phase transmission function by noting that

$|\phi(x,y)| = (2\pi/\lambda_0)\mathrm{OPD}(x,y)$, where $\phi(x,y)$ is the phase of the transmission function and OPD is the optical path difference introduced by the element. Also, $\mathrm{OPD} = [n(\lambda_0) - 1]d(x,y)$, where $n(\lambda_0)$ is the index of refraction at λ_0 and $d(x,y)$ is the thickness of the element at the point (x,y). Since the maximum phase modulation introduced by the kinoform is to be 2π, the maximum OPD introduced is λ_0. Thus, the maximum surface relief height $d_{\max}$ is

$$d_{\max} = \frac{\lambda_0}{n(\lambda_0) - 1}. \tag{3}$$

This is precisely the situation that has been analyzed by Dammann.[7] He shows that for a phase function, which we shall describe as

$$\phi(r) = \alpha 2\pi\left(m - \frac{r^2}{2\lambda_0 f}\right), \quad \text{for } r_m \le r < r_{m+1}, \tag{4}$$

a change of variables $\xi = r^2/(2\lambda_0 f)$ transforms the phase function into

$$\phi(\xi) = \alpha 2\pi(m - \xi), \quad \text{for } m \le \xi < m + 1. \tag{5}$$

In Eqs. (4) and (5), the parameter α is the fraction of 2π phase delay that is introduced for wavelengths other than the design wavelength λ_0. More specifically,

$$\alpha = \frac{\lambda_0}{\lambda}\frac{n(\lambda) - 1}{n(\lambda_0) - 1}. \tag{6}$$

The important observation about Eq. (5) is that now the transmission function $t(\xi) = \exp[i\phi(\xi)]$ is a periodic function of ξ and can be expanded as a Fourier series. The result is

$$t(\xi) = \exp[i\phi(\xi)] = \sum_{n=-\infty}^{\infty} c_n \exp(i2\pi n\xi), \tag{7a}$$

where

$$c_n = \frac{\exp[-i\pi(\alpha + n)]}{\pi(\alpha + n)} \sin[\pi(\alpha + n)]. \tag{7b}$$

Since we are assuming an implicit time dependence of $\exp(-i\omega t)$, a converging lens corresponds to a positive value of f in Eq. (1). We would like positive values of n to correspond to converging diffracted orders so that a positive order represents a positive lens. Therefore, we change n to $-n$ in Eqs. (7), reverse the order of summation, and make the reverse substitution for ξ. This gives

$$t(r) = \sum_{n=-\infty}^{\infty} \exp[-i\pi(\alpha - n)]\,\mathrm{sinc}(\alpha - n) \exp\left[\frac{-i\pi r^2}{\lambda_0(f/n)}\right], \tag{8}$$

where

$$\mathrm{sinc}(x) = \frac{\sin(\pi x)}{\pi x}. \tag{9}$$

From Eqs. (8) and (1) we see that this element behaves as a lens with an infinite number of focal lengths

$$f_{\text{kinoform}} = \frac{\lambda_0}{\lambda}\frac{f}{n}. \tag{10}$$

The efficiency in order n is given by

$$\eta = c_n c_n^* = \mathrm{sinc}^2(\alpha - n). \tag{11}$$

If $\alpha = 1$, i.e., if $\lambda = \lambda_0$, then $\eta = 1.0$ for $n = 1$ and is zero for all other orders. Thus, the element has a diffraction efficiency of 100% for the design wavelength. Dammann also considers the case when the desired parabolic profile is approximated by a series of discrete steps or sinusoids. Lenses using the discrete step approximation have been fabricated by several laboratories.[8,9]

Even though these elements are 100% efficient (for the design wavelength), good optical performance is limited to relatively high f/Nos. owing to the paraxial design. Comparing the corresponding terms in the transmission function and the phase terms in the binomial expansion of a spherical wave of radius $\zeta = \lambda_0 f/\lambda n$, i.e.,

$$\phi_{\text{sph}}(r) = \frac{2\pi}{\lambda}\left[\zeta - \sqrt{\zeta^2 + r^2}\right] = \frac{2\pi}{\lambda}\left(\frac{-r^2}{2\zeta} + \frac{r^4}{8\zeta^3} + \ldots\right), \tag{12}$$

or using the aberration model for diffractive optics developed by Sweatt[10] and Kleinhans,[11] we can calculate the amount of third-order wavefront spherical aberration for the first diffracted order of the paraxial design kinoform operating at infinite conjugates:

$$\pi_1(\lambda) = \frac{h}{(4f/\#)^3}\left(\frac{\lambda}{\lambda_0}\right)^3, \tag{13}$$

where h is the semiaperture of the element and $f/\#$ is the f/number defined as the ratio of the focal length to the clear aperture of the element. For third-order (primary) spherical aberration, the wavefront aberration polynomial has the form $W = \pi_1(\lambda)\rho^4$, where ρ is the normalized radial pupil coordinate.

To determine the optical performance of these devices, a computer program was written to calculate the point spread function (PSF) of a kinoform. The calculation is performed using a numerical implementation of the Huygens-Fresnel principle,[12] namely,

$$\Psi_{\mathrm{II}}(x,y,z) = \frac{-i}{\lambda}\int_{-\infty}^{\infty}\int_{-\infty}^{\infty} \Psi_{\mathrm{I}}(\xi,\eta,0)\frac{\exp(ikR)}{R} X(\theta)d\xi d\eta, \tag{14}$$

where $k = 2\pi/\lambda$, $X(\theta) = \cos(\theta)$ is the inclination factor, θ is the angle between the refracted ray and the observation point, and R is the propagation distance, $R = [(x - \xi)^2 + (y - \eta)^2 + z^2]^{1/2}$, in which z is the axial distance between the kinoform and the observation plane. In Eq. (14), Ψ_{I} is the scalar field in the kinoform plane and Ψ_{II} is the field in the observation plane.

It is interesting to point out here why we chose to perform the numerical integration of Eq. (14) to calculate diffraction patterns, rather than make use of the computational efficiency of fast Fourier transform (FFT) routines. When solving diffraction problems, one is usually presented with integrals of the form given by Eq. (14). These integrals can result from the use of the Huygens-Fresnel principle or a Rayleigh-Sommerfeld formula, based on the solution of the Helmholtz equation. In either case, we have a term of the form $\exp(ikR)$ in the integrand. The usual Fresnel approximation is to expand R in a binomial series and retain only terms up to second order, i.e.,

$$R_{\text{Fres}} = z + \frac{x^2 + y^2 + \xi^2 + \eta^2 - 2x\xi - 2y\eta}{2z}. \tag{15a}$$

Thus, in the Fresnel approximation, the diffraction integral takes the form

$$\Psi_{II_{Fres}}(x,y,z) = \frac{-i \exp\left[ikz + \frac{ik}{2z}(x^2+y^2)\right]}{\lambda z} \times \mathbf{FT}\left\{\Psi_I(\xi,\eta,0)X(\theta)\exp\left[i\frac{\pi}{\lambda z}(\xi^2+\eta^2)\right]\right\}, \tag{15b}$$

where **FT** indicates a Fourier transform and the frequency variables are given by $f_\xi = x/(\lambda z)$ and $f_\eta = y/(\lambda z)$. In Eq. (15b) we have also made the approximation $1/R \approx 1/z$. Equation (15b) is now in a form for which FFT techniques are suitable. However, the use of the Fresnel approximation has reduced the range of validity of the calculation to the paraxial region. We are interested in a more precise, nonparaxial calculation. We can try to increase the accuracy of the calculation and still retain the Fourier transform form of the integral by writing.

$$\exp(ikR) = \exp\left[\frac{-i2\pi}{\lambda z}(x\xi + y\eta)\right]\exp\left[\frac{+i2\pi}{\lambda z}(x\xi + y\eta)\right]\exp(ikR). \tag{16}$$

Then, Eq. (13) takes the form

$$\Psi_{II}(x,y,z) = \frac{-1}{\lambda z}\mathbf{FT}\{\Psi_I(\xi,\eta,0)X(\theta)\exp[ikR + i2\pi(f_\xi\xi + f_\eta\eta)]\}. \tag{17}$$

We still have a Fourier transform, but the function being transformed depends on the frequency variables. For every set of output coordinates (x,y), i.e., for every frequency pair (f_ξ,f_η), the transform would have to be recalculated. Since this eliminates the computational advantage of using FFT routines, we have chosen a direct numerical implementation of Eq. (14) to calculate diffraction patterns.

PSFs for $F/10$ and $F/5$ paraxial-designed kinoforms, both with a focal length of 50 mm, are shown in Fig. 1. For these calculations the reference wavelength λ_0 is chosen to be the helium-d line ($\lambda_0 = 0.58756\ \mu$m). The material for the kinoforms is PMMA (acrylic) plastic. The plots are calculated using an infinitely distant on-axis object, i.e., a normally incident plane wave. The intensity of each PSF is normalized such that the peak intensity of the PSF for the reference wavelength and an unaberrated diffracted wave is 1.0. At $F/10$, we see an Airylike pattern for the PSF, with a slightly reduced peak intensity due to a very small amount of spherical aberration. However, at $F/5$, the effect of retaining only the paraxial terms in designing the transmission function is evident, and the PSF is far from diffraction-limited. Even though this element is 100% efficient in diffracting all the incident light into one diffracted order, the resulting image in an $F/5$ element is highly aberrated.

III. Nonparaxial Kinoform Design

Our goal is to find a surface profile that retains the high diffraction efficiency of the parabolic blaze and also produces a high quality (unaberrated) diffracted wave. Our choice of profile is motivated by considering the exact expression in the x-y plane for the OPD of a converging spherical wave of radius f: OPD $= (f^2 + r^2)^{1/2} - f$. Consider a phase function of the form

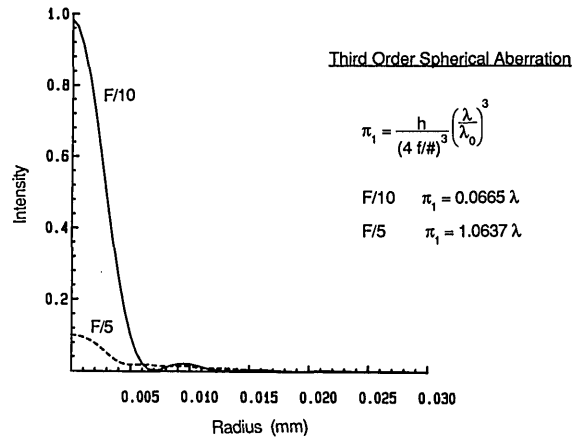

Fig. 1. Point spread functions for 50-mm focal length, paraxial design kinoforms. The solid line is an $F/10$ element; the dashed line is an $F/5$ element. Each curve is normalized such that the peak intensity for an unaberrated diffracted wavefront is 1.0.

$$\phi(r) = \alpha 2\pi\left(m - \frac{\sqrt{f^2+r^2} - f}{\lambda_0}\right), \quad \text{for } r_m \le r < r_{m+1}, \tag{18}$$

where the zone radius r_m is given in Eq. (2). Note that Eq. (4) is obtained by retaining only the first two terms of the binomial expansion of Eq. (18). If we make the change of variables $\xi = [(f^2 + r^2)^{1/2} - f]/\lambda_0$, Eq. (18) has the same form as Eq. (5). Now we have a 100% efficient element that produces a perfect spherical wave for the design wavelength. The profile of Eq. (18) is exactly the profile obtained from a variational analysis of zone plates[13] designed to maximize the intensity in the first-order diffraction focus. From the above discussion we see that the intensity is maximized because we have produced an unaberrated wavefront which contains all the incident energy. Performing a binomial expansion of the transmission function resulting from Eq. (18) {i.e., Eqs. (7) with $\xi = [(f^2 + r^2)^{1/2} - f]/\lambda_0$} and comparing the appropriate terms in the expansion of a perfect spherical wave [i.e., Eq. (12)] allow us to calculate the amount of third-order wavefront spherical aberration in the first diffracted order for the phase profile of Eq. (18):

$$\pi_1(\lambda) = \frac{h}{(4f/\text{No.})^3}\left(\frac{\lambda^3 - \lambda\lambda_0^2}{\lambda_0^3}\right). \tag{19}$$

Equation (19) shows that at $\lambda = \lambda_0$, $\pi_1(\lambda_0) = 0$. In fact, at the design wavelength, all orders of spherical aberration are zero. Again, the efficiency is given by $\eta = \text{sinc}^2(\alpha - n)$. PSFs calculated using the surface profile dictated by Eq. (18) are shown in Fig. 2. One can see that the PSF is essentially diffraction-limited for the range of apertures considered here.

It is worth pointing out that the resolution of the manufacturing process used to fabricate the kinoform determines the maximum feasible aperture. One can easily show that the minimum zone width s_{min} is given approximately by[8]

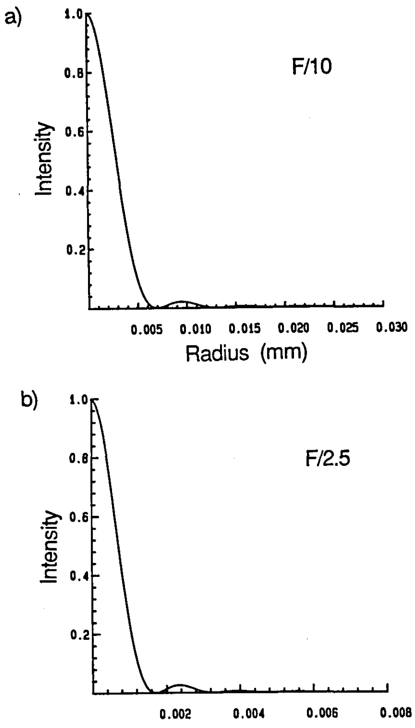

Fig. 2. Point spread functions for nonparaxial design kinoforms, $\lambda = \lambda_0 = 0.58756\ \mu m$; (a) $F/10$ kinoform; (b) $F/2.5$ kinoform.

$$s_{\min} = 2\lambda_0 f/\text{No.} \tag{20}$$

In the visible, $\lambda_0 \approx 0.5\ \mu m$, so $s_{\min} \approx f/\text{No.}\ \mu m$.

Both the paraxial and nonparaxial kinoforms described in this paper have been designed and evaluated using normally incident, plane wave illumination. Naturally, in optical systems, it may be required that the kinoforms operate at finite conjugate ratios. This shift of conjugates will change the amount of aberration introduced by both types of kinoform. Also, the kinoform substrate material, acting as a plane-parallel plate, will introduce aberrations at finite conjugates. Both of these effects should be taken into account in the design of any optical system which contains kinoform elements. Alternatively, if the conjugate ratio at which the kinoform is to operate is known, the zone spacing and blaze can be designed as to be correct for the two conjugate points.

We now consider the wavelength dependence of kinoforms. Again, there are two performance features that are wavelength dependent: diffraction efficiency and aberrations. The diffraction efficiency for order n, for both paraxial and nonparaxial designs, is given by Eq. (11). A plot of diffraction efficiency as a function of wavelength for orders $n = 0, 1$, and 2 is given in Fig. 3. As pointed out earlier and as is evident from the figure, $\eta = 1.0$ for the first diffracted order when used at the design wavelength λ_0.

The point spread functions for wavelengths other than the design wavelength will differ from the diffraction limit because of lower efficiency and aberrations. An efficiency <100% will reduce the amount of energy

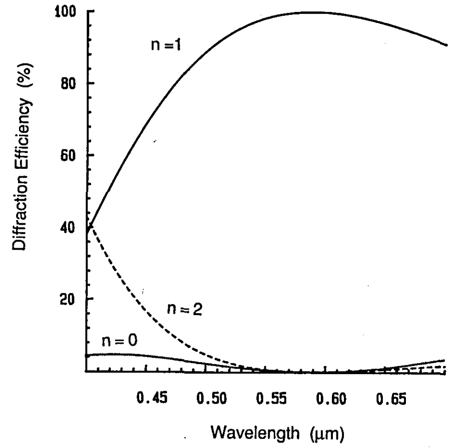

Fig. 3. Diffraction efficiency as a function of wavelength for diffracted orders $n = 0, 1$, and 2. The design wavelength is $\lambda_0 = 0.58756\ \mu m$. Note that $\eta = 1.0$ for $n = 1$ and $\lambda = \lambda_0$.

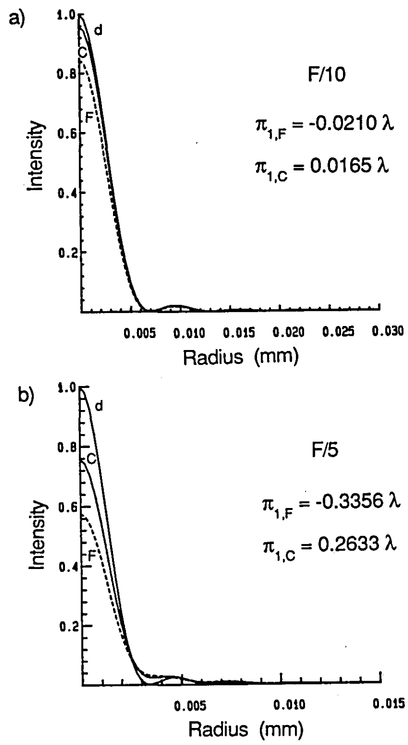

Fig. 4. Point spread functions for nonparaxial design kinoforms for three wavelengths. Each PSF was calculated in the paraxial focal plane for the wavelength of interest; (a) $F/10$ kinoform; (b) $F/5$ kinoform.

that is being focused to the focal plane for the diffracted order of interest, which is $n = 1$ in this case. The variation of spherical aberration with wavelength (spherochromatism) degrades the wavefront (to third order) by the amount given by Eq. (19). The PSFs for the helium-d, and hydrogen-F and C lines ($\lambda_F = 0.48613\ \mu m$; $\lambda_C = 0.65627\ \mu m$) for $F/10$ and $F/5$ systems are shown in Fig. 4. The point spread function for each wavelength was calculated in the paraxial focal plane for that wavelength. Obviously, in any broad-

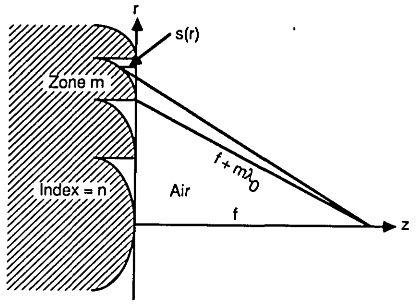

Fig. 5. Geometry and notation for the design of a finite thickness kinoform.

band system, the large amount of chromatic aberration must be corrected in the overall system design, since a single kinoform cannot be achromatized all by itself.

IV. Finite Thickness Kinoform Design

Thus far, we have ignored the fact that the diffracting surface of the kinoform has some finite thickness, which will affect the phase modulation introduced by the device. It is possible to take account of this finite thickness and the refraction of the light at the curved zone surface in the specification of the surface profile. Instead of working from the desired phase modulation, we use Fermat's principle to design the blaze such that the optical path length from any point in a given zone to the focal point is the same. Obviously, from zone to zone, the target optical path length will increase by one design wavelength, λ_0. This process is similar to the design of a refracting surface which equates optical path lengths to produce a stigmatic imaging system for a given pair of conjugate points. The calculation is set up as in Fig. 5. The sagitta of the surface is to be calculated so that the optical path length in the mth zone is the same from any incident position in that zone. The zone boundaries are given by the exact expression of Eq. (2). To equate the optical path lengths we set

$$-n(\lambda_0)s(r) + (f + m\lambda_0) = \sqrt{[f - s(r)]^2 + r^2}. \tag{21}$$

We want to solve Eq. (21) for $s(r)$, the sagitta (or sag) of the diffracting surface. Note that $s(r)$ is the directed distance from the tangent plane to the surface; this accounts for the negative sign of the first term on the left-hand side of Eq. (21). Equation (21) can be manipulated into the form

$$\frac{[s(r) - s_0]^2}{a^2} - \frac{r^2}{b^2} = 1, \tag{22}$$

where

$$s_0 = \frac{n(\lambda_0)[f + m\lambda_0] - f}{n^2(\lambda_0) - 1}, \tag{23a}$$

$$a^2 = \frac{[n(\lambda_0)f - f - m\lambda_0]^2}{[n^2(\lambda_0) - 1]^2}, \tag{23b}$$

$$b^2 = \frac{[n(\lambda_0)f - f - m\lambda_0]^2}{n^2(\lambda_0) - 1}. \tag{23c}$$

Thus we see that in each zone the proper surface is a hyperboloid of revolution, with eccentricity

$$e = \frac{\sqrt{a^2 + b^2}}{a} = n(\lambda_0). \tag{24}$$

We can recast Eq. (22) into a form similar to the standard optical design sag formula:

$$s(r) = \frac{m\lambda_0}{n(\lambda_0) - 1} + \frac{cr^2}{1 + \sqrt{1 - (\kappa + 1)c^2r^2}}. \tag{25}$$

In Eq. (25), c and κ are constants that define the paraxial curvature and conic constant, respectively. Explicitly, these parameters are given by

$$c = \frac{1}{f[1 - n(\lambda_0)] + m\lambda_0}, \tag{26a}$$

$$\kappa = -n^2(\lambda_0). \tag{26b}$$

The first term on the right-hand side of Eq. (25) is just the necessary correction so that the sag will go to zero at the edge of each zone. [Recall that $s(r)$ defines the surface sag relative to the tangent plane.] If we solve for the surface profile dictated by the thin, nonparaxial design, Eq. (18), by using $\phi(r) = (2\pi/\lambda_0)[n(\lambda_0) - 1]s_{\text{thin}}(r)$, we find that $s_{\text{thin}}(r)$ has the same functional form as Eq. (25), but the parameters c and κ are given as

$$c_{\text{thin}} = \frac{1}{f[1 - n(\lambda_0)]}, \tag{27a}$$

$$\kappa_{\text{thin}} = -[n(\lambda_0) - 1]^2 - 1. \tag{27b}$$

Comparing Eqs. (26) and (27), we see that taking account of the finite thickness of the element has dictated only slight modifications to the surface profile. The exact profile has a different paraxial curvature in each zone and a slightly different conic constant that is unchanging from zone to zone. It is well known[14] that the refracting surface, which will in the limit of geometrical optics form a perfect image of an infinitely distant on-axis point, is a hyperboloid of revolution with $c = 1/\{f[1 - n(\lambda_0)]\}$ and $\kappa = -n^2(\lambda_0)$. Thus, we see that the profile of Eqs. (25) and (26) is a combination of these perfect imaging hyperboloids, with different paraxial curvatures (and hence, different paraxial focal lengths) to account for the removal of the excess 2π phase modulations. These surfaces can be thought of as shells which intersect the optical axis at different points. Practically speaking, the differences between the profiles of Eqs. (26) and (27) are very slight, and only become significant at f/Nos. at which the precision of fabrication probably becomes the limiting factor.

V. Modeling of Kinoforms in Optical Design Software

Conventional optical design software programs are based on the tracing of exact rays through an optical system. The complex surface of a kinoform makes ray tracing more difficult than for a conventional, continuous optical surface. Also, since a typical kinoform consists of hundreds of diffracting zones, many more rays need to be traced than for conventional optics.

Another potential problem is the specification of the surface of the kinoform in a manner that the design program can recognize. Our goal is to develop a model for the imaging properties of a kinoform which is easily implemented into existing design programs.

Sweatt[10] has shown that, for any diffracted order, the first-order imaging properties and the third-order aberrations of a holographic lens are correctly modeled by an ultrahigh index lens. The equivalent model lens for an optically recorded HOE has surface specifications such that the element is corrected for spherical aberration for the conjugates at which the hologram was fabricated, with the additional requirement that the bending of the lens is determined by the substrate curvature. These model lenses have the property that all rays from the object source point travel through the model lens in a direction which is perpendicular to the HOE substrate. Since all the kinoforms described in this paper are planar elements—designed for use with an infinitely distant object, the equivalent ultrahigh index lens is plano–convex, with the curvature of the convex side determined such that the focal length is the desired value. If the index of the equivalent lens for the design wavelength λ_0 is $n_s(\lambda_0)$, the proper curvature is

$$c = \frac{1}{f[1 - n_s(\lambda_0)]} \cdot \tag{28}$$

As has been shown in the previous sections, the paraxial and nonparaxial design kinoforms have identical first-order properties, but different aberration properties. The choice of model lens surface curvature given by Eq. (28) determines the paraxial focal length and the aberration contributions associated with a spherical surface. We must specify the asphericity, if any, of this surface such that the total aberration introduced by the equivalent lens is the same as that of the kinoform. Thus, the aspheric deformation of this surface of the equivalent lens is determined from the specification of the zone locations,[11] as we have seen that the choice of paraxial or exact zone spacing determines the amount of geometrical aberration introduced by the kinoform. Generally, optical design programs require the description of a rotationally symmetric aspheric surface in terms of the conic constant (which is equal to the negative of the square of the eccentricity), if the asphere is a conic section, or in terms of the coefficients of a polynomial expression for the difference in sagitta between the asphere and a base sphere for a general rotationally symmetric asphere.

Comparing the aberration coefficients derived from the appropriate kinoform transmission functions [Eq. (13) for the paraxial design; Eq. (19) for the nonparaxial design] with those of an ultrahigh index lens, we can find the necessary aspheric deformation terms for the lens models of the two types of kinoform. (See any book on geometrical optics for a discussion of the aberrations of thin lenses and aspheric surfaces; for example, Ref. 15.) To find the appropriate coefficients, we compare terms in the expansions of the phase functions of the paraxial and nonparaxial design kinoforms with the aberration coefficients of a thin lens with one (possibly) aspheric surface when the index of refraction approaches infinity. The equality of the aberration coefficients requires that for a paraxial design, all aspheric coefficients of the convex surface are zero, whereas for the nonparaxial design, the conic constant is $\kappa = -n_s^2(\lambda_0)$. To account for the chromatic variation of focal length, indicated by Eq. (10), the refractive index of the ultrahigh index material, $n_s(\lambda)$, is made linearly proportional to wavelength. Finally, we note that in all realistic planar kinoforms the surface relief profile will be on one side of a plane-parallel substrate. One can easily show that a plane-parallel plate will introduce aberrations if used at finite conjugates.[16] To account for this, the ultrahigh index lens should be placed in contact with a plane-parallel slab of the material of which the kinoform is made, with a thickness equal to the kinoform substrate thickness. The refractive-index properties of this plate will be those of the kinoform material, not the ultrahigh index lens model material.

The model described above will correctly predict the location and aberrations of a kinoform-produced image, but not the energy distribution among the various diffracted orders. Also, the multiplicity of images resulting from the different orders has been ignored, since a refractive lens produces only one image. If it is desired to calculate point spread functions, or other diffraction-based image parameters, the diffraction efficiency of the kinoform must be considered. Ignoring the effects of aberrations by using the Fresnel approximation to the Huygens-Fresnel integral, i.e., Eq. (15), we can predict the form of a perfect point spread function. The relative values of peak diffracted intensity, for an on-axis observation point, for each wavelength calculated from the Fresnel theory can be used as spectral weighting factors for the wavelengths used in the design program, so that the relative peak diffraction intensities computed by the design program match those of the Huygens-Fresnel theory. This weighting reflects the diffraction efficiency in the order of interest but ignores the background illumination resulting from the other diffracted orders. Thus, the diffraction patterns calculated by this model include only the energy diffracted into the order of interest. If the amount of background illumination, i.e., light diffracted into other orders, is large, this model will become more inaccurate. This will occur for wavelengths further removed from the design wavelength, i.e., for values of α significantly different from unity [see Eq. (6)]. (It should be noted that the predictions of scalar diffraction theory become increasingly inaccurate at extremely high apertures,[17] but the differences between the Huygens-Fresnel calculation and a more exact vector calculation are negligible for relative apertures such that the f/No. is greater than $\sim F/0.9$, which includes all the elements considered in this paper.) In the Fresnel approximation, we can calculate explicity the on-axis intensity produced by a kinoform for a normally incident plane wave. This is done by using the transmission function resulting from

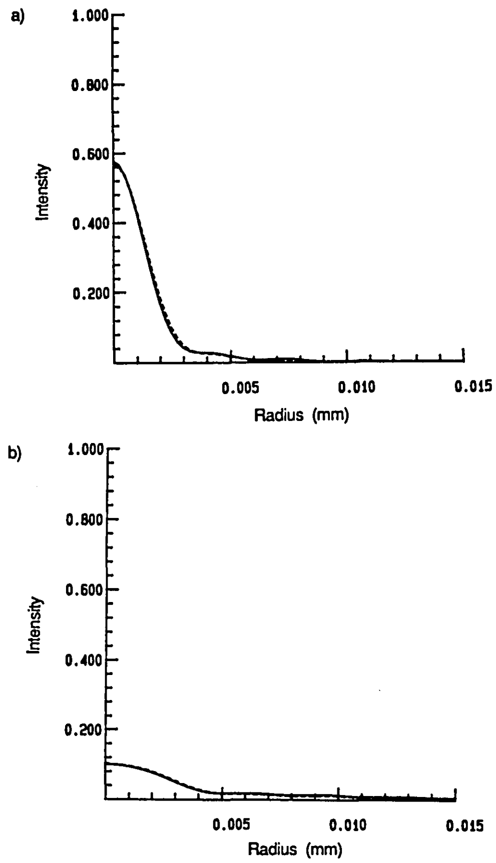

Fig. 6. Comparison of Huygens-Fresnel and ultrahigh index model calculations of point spread functions. The solid line is the Huygens-Fresnel result and the dashed line is the ACCOS V calculation; (a) nonparaxial design, $F/5$ kinoform, $\lambda = 0.48613\ \mu$m (hydrogen-F line); (b) paraxial design, $F/5$ kinoform, $\lambda = \lambda_0 = 0.58756\ \mu$m.

Eq. (4) in the Fresnel diffraction integral, Eq. (15), with $x = y = 0$ to find the on-axis field produced by one diffracting zone. The result is then summed over all the zones to find the total on-axis diffracted field. The on-axis intensity $I(0,0,z)$, normalized at the first-order diffraction focal point for $I(0,0,f) = 1.0$ when $\lambda = \lambda_0$, is

$$I(0,0,z) = \frac{\sin^2\left(\frac{\pi\lambda_0 f N}{\lambda z}\right)}{(\pi N)^2\left(1 - \frac{\alpha\lambda z}{\lambda_0 f}\right)^2}\left\{\cos(\alpha\pi) - \frac{\sin(\alpha\pi)}{\tan[(\pi\lambda_0 f)/(\lambda z)]}\right\}^2. \quad (29)$$

In Eq. (29), N is the number of zones in the kinoform. At a focus, $z_{\text{focus}} = (\lambda_0 f)/(\lambda n)$ (f is the design focal length for $\lambda = \lambda_0$, and n is the diffracted order), and Eq. (29) reduces to

$$I\left(0,0,\frac{\lambda_0 f}{\lambda n}\right) = n^2 \operatorname{sinc}^2(\alpha - n) = n^2\eta. \quad (30)$$

Equation (30) indicates that we should spectrally weight the different wavelengths by an amount proportional to the diffraction efficiency times the square of the order number n. In most cases, we will be concerned with the first diffracted order ($n = 1$), so the wavelengths will be weighted by their relative diffraction efficiency. The efficiency can be calculated from Eq. (11) for the wavelengths of interest.

As examples of the accuracy of this model, results from the Huygens-Fresnel calculation were compared to point spread functions calculated, using the model, by ACCOS V,[18] a commercial lens design program. In Fig. 6, we see that the different procedures produce very similar results. We would expect the model to give erroneous results for wavelengths where the parameter α is sufficiently different from one. If this is the case, the background intensity due to the other orders could not be ignored.

VI. Summary

Kinoforms can serve as high efficiency, diffractive optical elements and can produce high quality wavefronts. It is necessary to use a nonparaxial design for good results when working at f/Nos. less than $\sim F/10$. The wavelength dependence of both diffraction efficiency and aberrations must be considered when kinoforms are to be used in an optical system. It is possible to model kinoforms as ultrahigh index lenses in design programs, so optical systems containing these elements can be evaluated.

The authors gratefully acknowledge the support of this research by DARPA, the MIT/Lincoln Laboratory, and 3M Company. D. A. Buralli acknowledges the support of the Kodak Fellows Program.

Portions of this work were presented as paper 883-07 at the SPIE O-E/LASE '88 Conference, Los Angeles, CA, 10–17 Jan. 1988.

References

1. L. B. Lesem, P. M. Hirsch, and J. A. Jordan, Jr., "The Kinoform: a New Wavefront Reconstruction Device," IBM J. Res. Dev. **13**, 150 (1969).
2. J. A. Jordan, Jr., P. M. Hirsch, L. B. Lesem, and D. L. Van Rooy, "Kinoform Lenses," Appl. Opt. **9**, 1883 (1970).
3. G. G. Sliusarev, "Optical Systems with Phase Layers," Sov. Phys. Dok. **2**, 161 (1957).
4. A. I. Tudorovskii, "An Objective with a Phase Plate," Opt. Spectrosc. **6**, 126 (1959).
5. K. Miyamoto, "The Phase Fresnel Lens," J. Opt. Soc. Am. **51**, 17 (1961).
6. J. W. Goodman, *Introduction to Fourier Optics* (McGraw-Hill, New York, 1968), pp. 77–83.
7. H. Dammann, "Blazed Synthetic Phase Only Holograms," Optik **31**, 95 (1970).
8. L. d'Auria, J. P. Huignard, A. M. Roy, and E. Spitz, "Photolithographic Fabrication of Thin Film Lenses," Opt. Commun. **5**, 232 (1972).
9. G. J. Swanson and W. B. Veldkamp, "Binary Lenses for Use at 10.6 Micrometers," Opt. Eng. **24**, 791 (1985).
10. W. C. Sweatt, "Describing Holographic Optical Elements as Lenses," J. Opt. Soc. Am. **67**, 803 (1977).
11. W. A. Kleinhans, "Aberrations of Curved Zone Plates and Fresnel Lenses," Appl. Opt. **16**, 1701 (1977).
12. M. Born and E. Wolf, *Principles of Optics* (Pergamon, Oxford, 1980), pp. 370–375.
13. R. Tatchyn, P. Csonka, and I. Lindau, "A Unified Approach to the Theory and Design of Optimum Transmission Diffraction Systems in the Soft X-Ray Range," Proc. Soc. Photo-Opt. Instrum. Eng. **503**, 168 (1984).

14. R. Kingslake, *Lens Design Fundamentals* (Academic, Orlando, 1978), pp. 112–113.
15. W. T. Welford, *Aberrations of Optical Systems* (Adam Hilger, Bristol, 1986), pp. 152–153 and 226–234.
16. Ref. 15, pp. 234–235.
17. See, for example, H. H. Hopkins, "The Airy Disk Formula for Systems of High Relative Aperture," Proc. Phys. Soc. London **55**, 116 (1943); M. Mansuripur, "Distribution of Light at and Near the Focus of High-Numerical-Aperture Objectives," J. Opt. Soc. Am. A **3**, 2086 (1986).
18. ACCOS V is a trademark of Scientific Calculations, Inc., 7635 Main St., Fishers, New York 14453.

Meetings *continued from page 864*

1989
August

20–25 9th Int. Conf. on Crystal Growth, Sendai *Secretariat: 9th Int. Conf. on Crystal Growth, c/o Inter Group Corp., 8-5-32 Akasaka, Minato-ku, Tokyo 107, Japan*

22–26 10th Int. Symp. on Nuclear Quadrupole Resonance Spectroscopy, Takayama *T. Asaji, Dept. of Chem., PC 11, Faculty of Science, Nagoya U., Chikusa, Nagoya 464-01, Japan*

26–31 7th Int. Summer School on Crystal Growth, Zao *H. Komatsu, Inter Group Corp., Akasaka Yamakatsu Bldg., 8-5-32 Akasaka, Minato-ku, Tokyo 107, Japan*

27–31 3rd Int. Symp. on Foundation of Quantum Mechanics—In the Light of New Tech., Tokyo *H. Ezawa, Dept. of Physics, Gakushuin U., Mejiro, Toshima-ku, Tokyo 171, Japan*

28–31 7th Int. Conf. on Dynamical Processes in Excited States of Solids, Athens, GA *J. Rives, Physics & Astronomy Dept., U. of GA, Athens, GA 30602*

September

4–8 ISES Solar World Congress, Kobe *Secretariat, Int. Communications, Inc., Kasho Bldg., 2-14-9 Nihonbashi, Chuo-ku, Tokyo 103, Japan*

5–8 O-E/Fibers '89 Symp. Optoelectronics & Fiber Optic Devices & Applications, Boston *SPIE, P.O. Box 10, Bellingham, WA 98227*

9–14 2nd Int. Symp. on Rare Earth Spectroscopy, Changchun *S. Qiang, Changchun Inst. of Applied Chem., Academia Sinica, Changchun 130022, China*

11–15 European Conf. on Optical Communication, Gothenberg *ECOC '89, Chalmers U. of Tech., S-41296 Gothenberg, Sweden*

14–16 Int. Symp. on Noise & Clutter Rejection in Radar & Imaging Sensors, Kyoto *T. Suzuki, Dept. of Electronics, U. of Electro-Communications, Chofu-shi, Tokyo 182, Japan*

23–29 Advanced Processing Tehnologies for Optical & Electronic Devices Mtg., Santa Clara *SPIE, P.O. Box 10, Bellingham, WA 98227*

25–29 Int. Conf. on Solid Surfaces. Cologne *A. Benninghoven, Physikalisches Institut der Universitat Munster, Wilhem-Klemm-Strasse 10, D-4000 Munster, F.R. Germany*

25–29 16th Int. Symp. on Gallium Arsenide & Related Compounds, Karuizawa *T. Katoda, Res. Center for Advanced Science & Tech., U. of Tokyo, 4-6-1 Komaba, Meguro-ku, Tokyo 153, Japan*

26–28 Int. Symp. on Optical Memory, Kobe *Secretariat, c/o Business Center for Academic Societies Japan, 3-23-1 Hongo, Bunkyo-ku, Tokyo 113, Japan*

26–29 3rd Int. Conf. on Laser Anemometry Advances & Applications, Wales *L A Conf. 1989, Dept. of Engineering, U. of Manchester, Manchester M13 9PL, England*

29–30 Innovation Workshops, Ames *Off. of Energy-Related Inventions, NIST, 209 Eng. Mechanics Bldg., Gaithersburg, MD 20899*

October

7–10 7th Int. Congr. Applications of Lasers & Electrooptics, Boston *Laser Inst. Am., 5151 Monroe St., Toledo, OH 43623*

15–20 **Optics '89: OSA Ann. Mtg., Orlando** *OSA Mtgs. Dept., 1816 Jefferson Pl., NW, Wash., DC 20036*

18–21 Pacific Conf. on Chemistry & Spectroscopy, Pasadena *W. Carter, P.O. Box 5732, Pasadena, CA 91107*

22–26 Int. Conf. on Semiconductor & Integrated Circuit Tech., Beijing *Cont. Ed. in Eng., U. Ext., U. of CA, 2223 Fulton St., Berkeley, CA 94720*

November

5–10 1989 Advances in Intelligent Robotics Systems, Philadelphia *SPIE, P.O. Box 10, Bellingham, WA 98227*

7–10 36th AVS Natl. Vacuum Symp., Phoenix *AVS, 335 E. 45th St., New York, NY 10017*

9–11 Optical Storage for Small Systems Mtg., Los Angeles *TOC, P.O. Box 14817, San Francisco, CA 94114*

12–17 5th Int. Congr. on Advances in Non-Impact Printing Technologies, San Diego *SPSE, 7003 Kilworth La., Springfield, VA 22151*

continued on page 1014